energies

MDPI

Article

Hydrothermal Liquefaction of Sugarcane Bagasse and Straw: Effect of Operational Conditions on Product Fractionation and Bio-Oil Composition

Raquel Santos Silva [1,2], Reinaldo Alves da Silva, Jr. [1,2], Flávio Montenegro de Andrade [2,3], Pedro Nunes Acácio Neto [1,2], Rayane Maria do Nascimento [4], Jandyson Machado Santos [4], Luiz Stragevitch [1,2], Maria Fernanda Pimentel [1,2], Diogo Ardaillon Simoes [2,5] and Leandro Danielski [1,2,*]

1 Department of Chemical Engineering, Federal University of Pernambuco, Av. dos Economistas, s/n, Recife 50740-590, Brazil
2 Fuel Laboratory (LAC), Institute for Petroleum and Energy Research (i-LITPEG), Federal University of Pernambuco, Av. da Arquitetura, s/n, Recife 50740-550, Brazil
3 Department of Fundamental Chemistry, Federal University of Pernambuco, Av. Jorn. Aníbal Fernandes, s/n, Recife 50740-560, Brazil
4 Department of Chemistry, Federal Rural University of Pernambuco, Rua Manuel de Medeiros, s/n, Recife 52171-900, Brazil
5 Department of Biochemistry, Federal University of Pernambuco, Av. Reitor Joaquim Amazonas, s/n, Recife 50740-570, Brazil
* Correspondence: leandro.danielski@ufpe.br

Abstract: In the energy transition process, aiming for zero disposal and clean production in the elimination of waste is crucial; consequently, agricultural residues have significant potential for reduction in the use of fossil fuels. This study investigates the hydrothermal liquefaction (HTL) of sugarcane bagasse (BSC) and straw (SSC), examining the products' distribution and bio-oil composition relative to the reaction conditions. The experiments used a 2^3 factorial design, evaluating the temperature (300–350 °C), constant heating time (0–30 min), and the use of the K_2CO_3 concentration as the catalyst (0–0.5 mol/L^{-1}). The main factor affecting the biocrude yield from BSC and SSC was the use of K_2CO_3. Statistically significant interaction effects were also observed. Milder conditions resulted in the highest bio-oil yields, 36% for BSC and 31% for SSC. The catalyst had no impact on the biocrude production. The bio-oils were analyzed by GC/MS and FTIR; a principal component analysis (PCA) was performed to evaluate the samples' variability. The FTIR highlighted bands associated with common oxygenated compounds in lignocellulosic biomass-derived bio-oils. The GC-MS results indicated a predominance of oxygenated compounds, and these were highest in the presence of the catalyst for both the BSC (90.6%) and SSC (91.7%) bio-oils. The SSC bio-oils presented higher oxygenated compound contents than the BSC bio-oils. Statistical analysis provided valuable insights for optimizing biomass conversion processes, such as determining the optimal conditions for maximizing product yields.

Keywords: biomass conversion; hydrothermal liquefaction; HTL; residues; bio-oil; statistical treatment

check for updates

Citation: Silva, R.S.; da Silva, R.A., Jr.; de Andrade, F.M.; Acácio Neto, P.N.; do Nascimento, R.M.; Santos, J.M.; Stragevitch, L.; Pimentel, M.F.; Simoes, D.A.; Danielski, L. Hydrothermal Liquefaction of Sugarcane Bagasse and Straw: Effect of Operational Conditions on Product Fractionation and Bio-Oil Composition. *Energies* **2024**, *17*, 5439. https://doi.org/10.3390/en17215439

Academic Editor: Marcin Dębowski

Received: 3 October 2024
Revised: 22 October 2024
Accepted: 29 October 2024
Published: 31 October 2024

Copyright: © 2024 by the authors. Licensee MDPI, Basel, Switzerland. This article is an open access article distributed under the terms and conditions of the Creative Commons Attribution (CC BY) license (https://creativecommons.org/licenses/by/4.0/).

1. Introduction

As the global economy and population continue to grow, the demand for the planet's energy resources continues to rise. The acquisition of these resources can be expensive and challenging due to their scarcity or environmental risks. Consequently, there is significant interest in generating energy from sources that are accessible, environmentally sustainable, and renewable. Among the sources of renewable energy, biomass is one of the most promising feedstocks [1].

Biomass is the third primary renewable energy source worldwide and is mainly composed of carbon, hydrogen, oxygen, and nitrogen. These elements are key components

for many processes [2], whether they are thermochemical, hydrothermal or biological. A variety of processes, including thermochemical ones like combustion, gasification, and pyrolysis, biological processes like biological conversion, and hydrothermal treatment processes such as carbonization, liquefaction, and gasification, can convert biomass into bioenergy (heat and power), biofuels, biochemicals, and other materials [3].

Additionally, bagasse and sugarcane straw are frequently burned in boilers to produce heat and electricity, playing a significant role in the energy matrix. However, it is crucial to consider energy densification: as examples, raw sugarcane bagasse (BSC) and straw (SSC) present higher heating values (HHV) of around 17 MJ/kg, while the bio-oils obtained from BSC and SSC may reach HHV values of approximately 33–36 MJ/kg, depending on the conditions evaluated. This substantial increase in the HHV of bio-oil relative to the corresponding biomass underscores its greater energy efficiency and density, highlighting its potential as a superior renewable fuel, particularly when considering the amount of energy stored per unit of mass [3,4].

Sugarcane is the base of a successful agro-industrial system that spans various tropical and subtropical regions worldwide. This industry is constantly evolving, aiming to diversify its range of products and utilize the abundant lignocellulosic raw materials that are available, such as bagasse and straw. These trends have transformed the sugarcane industry into a fundamental field of study for exploring the potential of agricultural residues and herbaceous biomass in bioenergy production and the development of biorefineries [4].

The techniques employed for the thermochemical conversion of biomass into energy have garnered significant interest within the scientific community and continue to be studied, as exemplified by Kumar et al. [5], who investigated the integration of hydrothermal carbonization and pyrolysis (HTC–PY). Given that hydrothermal conversion is suitable for various types of biomass feedstocks and offers advantages in terms of high efficiency and conversion rates [6], hydrothermal liquefaction (HTL) has emerged as a crucial thermochemical process for converting moisture-containing feedstocks into bioenergy and high-value-added products [7].

HTL can be integrated into sugarcane biorefineries to produce bio-oils from wet biomasses such as sugarcane bagasse, forest residues, and lignin-rich streams from second-generation ethanol production. The main advantage of biomass conversion over other methods is the potential for the use of wet biomass, thus avoiding the costs of drying, a mandatory step for pyrolysis or gasification processes, reducing the associated energy consumption [8,9].

In the hydrothermal liquefaction process (Figure 1), biomass is subjected to a reaction in hot water under high pressure. The pressure needs to be high enough to keep the water in a liquid or supercritical state. This process aims to break down solid biomass into mostly liquid components, with or without the presence of catalysts [10].

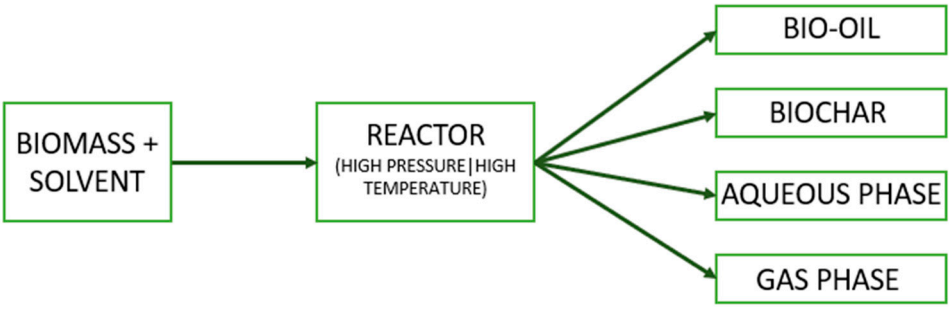

Figure 1. Schematic representation of the HTL process.

During the conversion of wet biomass via HTL, a cascade of reactions takes place, breaking down the macromolecules of organic material and resulting in four different products: bio-oil (a viscous dense dark liquid), a solid byproduct (biochar), a gaseous

stream, and an aqueous lighter phase rich in soluble organics [11,12]. These products can serve as alternatives to fossil resources and other non-renewable products [6].

The bio-oils produced by HTL can be used directly as substitutes for fossil fuels or as energy intermediates in the production of drop-in biofuels such as bio-gasoline, aviation bio-kerosene, and green diesel through gasification and Fischer–Tropsch synthesis processes [13].

Improving operational conditions is vital for increasing bio-oil yield and maximizing the potential of HTL in biorefineries. However, despite its remarkable characteristics, bio-oil also poses a significant challenge in terms of its optimization and subsequent processes due to its wide variety of chemical compounds, which may include linear and branched aliphatic compounds, aromatic and phenolic derivatives, carboxylic acids, esters, and nitrogen-containing ring structures [8,14–16].

This study contributes to advancing the knowledge in the field of the hydrothermal liquefaction (HTL) of agricultural residues, specifically sugarcane bagasse and straw. The comparative approach used in this study between these two biomaterials is unprecedented in the scientific literature. The application of multivariate statistical techniques has enabled the quantification of the effects of different operational variables, such as the temperature, constant heating time, and catalyst concentration under experimental conditions, as well as the assessment of the variability among the products obtained from bagasse and straw. This statistical approach not only highlights differences in the chemical compositions of the produced bio-oils, but also provides crucial insights for optimizing the lignocellulosic biomass conversion processes. Consequently, the present study fills a gap in the literature by exploring these comparisons, while simultaneously granting new perspectives for the development of sustainable biofuel production strategies.

2. Materials and Methods

2.1. Materials

BSC and SSC were obtained from the Brazilian Biorenewables National Laboratory (LNBR, Campinas, Brazil). All biomasses were subjected to grinding in a knife mill before use in the liquefaction experiments to reduce particle sizes to less than 0.84 mm. This is the same particle size used in the experiments of Yan et al. [17]. Using sugarcane bagasse, they studied the effect of different catalysts and process parameters on the chemical contents of bio-oils obtained from hydrothermal liquefaction. The ground material was stored in plastic packages and kept at room temperature. The compositions of the BSC and SSC cellulose, hemicellulose, lignin, ash, and extractives were characterized at the LNBR facilities and are shown in Table 1. Ashes, extractives, and insoluble lignin were analyzed by gravimetry, while soluble lignin was analyzed by spectrophotometry. The contents of carbohydrates (cellulose and hemicellulose) were determined by high-performance liquid chromatography (HPLC). Cellulose, hemicellulose, lignin, and extractives were analyzed in duplicates, while total ashes were determined once.

Table 1. Chemical composition of sugarcane bagasse and sugarcane straw.

Biomass	Values	Cellulose	Hemicellulose	Soluble Lignin	Insoluble Lignin	Extractives	Total Ash	MB *
Bagasse	Mean (%)	42.61	28.66	3.12	23.34	2.61	0.94	101.14
	SD ** (%)	0.51	0.46	0.32	0.36	0.52	n/a	0.21
Straw	Mean (%)	37.66	29.66	1.88	19.20	7.40	3.26	99.06
	SD ** (%)	1.18	0.14	0.20	0.20	0.26	n/a	1.05

* Mass balance, n/a: not applicable because it was not performed in duplicate. ** (SD) standard deviation.

2.2. Chemicals

Potassium carbonate (K_2CO_3; 98%) was obtained from Anidrol (Diadema/SP, Brazil), acetone (C_3H_6O; 99.5%) was obtained from Química Moderna (Barueri/SP, Brazil), and

the nitrogen gas (N_2; 99.999%) was purchased from Air Liquide (São Paulo/SP, Brazil). All chemicals and reagents were used as received without further purification. Distilled and deionized water (Merck deionizer, model Direct—Q3 UV, Darmstadt, Germany) was employed as the solvent.

2.3. Hydrothermal Liquefaction Experiments

The reactor vessel (Model 4576, Parr Instrument Company, Moline, IL, USA) was charged with a 1:9 ratio of ground biomass to solvent, using 12 g of biomass and 108 mL of solvent (either distilled and deionized water or a 0.5 mol/L^{-1} potassium carbonate solution). This established a biomass concentration of 10% (mass basis) in the reaction system, consistent with the values reported by Brand et al. [18] and Long et al. [19]. The reactor was sealed, purged three times with nitrogen gas to create an inert atmosphere, and pressurized to 50 bar. The temperature was adjusted to the desired levels of 300, 325, and 350 °C, as these values were selected based on evidence from Brand et al. [20], Caprariis et al. [21], and Mathanker et al. [22] which indicated that temperatures between 300 and 350 °C were more effective for maximum bio-oil yields. A heating rate of approximately 5 °C min^{-1} was used. The reactor contents were continuously stirred at 100 rpm.

In this work, the methodology used by Toor et al. [23] was adopted. Additionally, to reduce the heating ramp time interval, an electric resistance was attached externally to the reaction vessel. The constant heating time was defined as the duration for which the reactor temperature was maintained (0, 15, and 30 min), following Mathanker et al. [22] and Durak and Genel [24]. After the given constant heating time was reached, the heater was turned off and a stream of cold water was circulated through the reactor cooling coil.

After cooling, the reactor was depressurized to release the gas phase and opened to separate the liquid and solid phases. Samples of the gas phase were collected and stored in bags for analysis. Liquid and solid phases were separated in a vacuum filtration system. The filtrate was the aqueous phase, while the materials retained on the filter paper were the bio-oil and the solid residue. The walls of the reactor and its internal fittings were cleaned using cotton soaked in acetone. Filter paper and cotton swabs had been previously weighed to later measure biochar and bio-oil masses by difference.

To separate the bio-oil from the solid residue (biochar), a Soxhlet extractor was employed: filter cake, filter papers, and the cotton swabs used to clean the reactor were placed in a cartridge and subjected to a liquid–liquid extraction for 6–8 h at 60–80 °C using acetone as the solvent [22]. After extraction, the remaining solids were separated from the acetone solution and dried for 24 h at room temperature.

The extract, a solution of bio-oil in acetone, was placed in a rotary evaporator (Model MA-120, Marconi, Piracicaba, SP, Brazil) under a vacuum pressure of 150 mmHg and at 60 °C for about 2 h until all the acetone present in the extract was evaporated. Thus, the material remaining in the rotary evaporator flask was the bio-oil. The mass of the bio-oil was obtained by difference from the mass of the rotary evaporator flask, which was previously determined.

Based on the works of Mathanker et al. [22] and Singh et al. [25], conversion (X) and product yields (Y) were defined by Equations (1)–(5):

$$X(\%) = \frac{m_{biomass} - m_{solid\ residue}}{m_{biomass}} \times 100 \quad (1)$$

$$Y_{bio-oil}(\%) = \frac{m_{bio-oil}}{m_{biomass}} \times 100 \quad (2)$$

$$Y_{solid\ residue}(\%) = \frac{m_{solid\ residue}}{m_{biomass}} \times 100 \quad (3)$$

$$Y_{gas\ phase}(\%) = 1 - \frac{m_{bio-oil} + m_{solid\ residue} + m_{aqueous\ phase}}{m_{biomass} + m_{solvent}} \times 100 \quad (4)$$

$$Y_{aqueous\ phase}(\%) = 100 - m_{bio-oil} - m_{solid\ residue} - m_{gas\ phase} \quad (5)$$

where *m* stands for mass.

2.4. Experimental Design

A 2^3 factorial design with a central point was used to optimize bio-oil production in hydrothermal liquefaction experiments. The parameters evaluated were temperature (T), constant heating time (t), and catalyst concentration (C). The levels were chosen based on preliminary tests, as well as on methodologies previously published in the literature [22,26]. Jindal and Jha [26] have investigated the use of different catalysts at different concentrations and found that basic salt aqueous solutions generally exhibit higher catalytic activities than their corresponding hydroxides in HTL experiments with lignocellulosic biomass.

For each condition, experiments were repeated, including the central point, resulting in 18 experiments. Table 2 shows the levels selected for each variable in the design. The response evaluated was the bio-oil yield and the statistical analysis was performed using the Statistica software (version 10) at a confidence level of 95%.

Table 2. Levels adopted for experimental design in hydrothermal liquefaction.

Parameters	Levels		
	−1	**0**	**+1**
T (°C)	300	325	350
t (min)	0	15	30
C (mol/L^{-1})	0	0.25	0.5

2.5. Product Characterization

2.5.1. FTIR Data Acquisition

Bio-oil samples were characterized using Fourier-transform infrared spectroscopy (FTIR) to explore the generic functional groups. The spectra were acquired using a benchtop spectrometer (Spectrum 400, PerkinElmer, Waltham, MA, USA) with an attenuated total reflectance (ATR) accessory, wavenumber range from 4000 to 550 cm^{-1}, average of 32 scans, and resolution of 4 cm^{-1}.

2.5.2. Gas Chromatography Coupled to Mass Spectrometry (GC-MS)

Bio-oil samples with the highest yields obtained using BSC and SSC biomasses were analyzed by gas chromatography coupled to mass spectrometry (GC-MS). First, 5 mg of bio-oil was diluted in 10 mL of tetrahydrofuran (THF), with a final concentration of 0.5 mg/mL^{-1}. Then, 1 mL of the solution was derivatized with 110 µL of N,O-bis(trimethylsilyl)trifluoroacetamide (BSTFA) using a vial flask, which was subjected to 60 °C for 30 min in a drying oven. The GC-MS analyses were performed using a gas chromatograph/quadrupole mass spectrometer (GCMS-QP2010 SE, Shimadzu, Kyoto, Japan) coupled to an autosampler (AOC-6000 Plus, Shimadzu, Kyoto, Japan) operated with electron ionization (EI) at 70 eV, and a DB-5MS capillary column (60 m × 0.25 mm × 0.25 µm, PerkinElmer, Waltham, MA, USA). A volume of 1 µL of the derivatized solution was injected in splitless mode, and the injector temperature was set at 280 °C. Helium was used as the carrier gas at a column flowrate of 0.95 mL/min^{-1}. The oven temperature was initially set at 60 °C for 4 min, followed by a ramp-up of 4 °C min^{-1} to 300 °C, which was held for an additional 10 min. The MS was set for scanning the mass range from 50 to 550 Da. The data were acquired and processed using the GCMSsolution software (v. 4.20, Shimadzu, Kyoto, Japan) and compound identification was performed by comparing the mass spectrometry data with the NIST5, NIST5s, and NIST21 libraries. Assignments with a similarity higher than 75% were considered for correspondence.

2.5.3. Chemometric Analysis

A principal component analysis (PCA) was performed using the FTIR spectral data. Some pre-processing techniques had been previously evaluated to reduce the physical effects present in the spectra. Among these, the standard normal variate (SNV), the multiplicative scatter correction (MSC), and the first derivative with Savitzky–Golay smoothing filter were evaluated using different window sizes. Prior to the modeling step, the pre-processed spectra were mean-centered. The chemometric analysis was carried out with PCA models built using the PLS Toolbox (version 9.3, Eigenvector Research Inc., Manson, WA, USA), using Matlab software (MATLAB R2010a 7.10.0.499, MathWorks Inc., Natick, MA, USA).

3. Results

HTL experiments were performed using the described methods and the obtained results are presented and discussed below.

3.1. Hydrothermal Liquefaction Results

To simplify identification, the experiments were labeled based on the resulting biomass, temperature, constant heating time, and catalyst presence. The parameters were represented by their initials and values. For example, BSC300-30C denotes the experiment with BSC at 300 °C, for 30 min, and with a catalyst (K_2CO_3), while SSC350-0 denotes SSC at 350 °C, for 0 min, and with no catalyst.

3.1.1. Results of the 2^3 Factorial Design

Table 3 presents the results of the yields (response) obtained in each experimental condition.

Table 3. Design matrix and obtained responses for the experimental designs of hydrothermal liquefaction with the two biomasses.

EXP.	Levels			BSC		SSC	
	T	t	C	Yield (%)	Mean (%)	Yield (%)	Mean (%)
1	−1	−1	−1	37.6 | 35.1	36.4	32.4 | 29.3	30.9
2	+1	−1	−1	33.8 | 32.3	33.1	26.4 | 27.3	26.9
3	−1	+1	−1	35.2 | 33.1	34.2	31.7 | 30.1	30.9
4	+1	+1	−1	32.7 | 29.3	31.0	30.4 | 27.7	29.1
5	−1	−1	+1	16.0 | 17.9	17.0	17.1 | 12.6	14.9
6	+1	−1	+1	20.8 | 22.0	21.4	22.6 | 19.1	20.9
7	−1	+1	+1	20.7 | 21.2	20.1	17.7 | 16.7	17.2
8	+1	+1	+1	19.4 | 20.9	20.2	17.1 | 16.9	17.0
9	0	0	0	25.0 | 26.7	25.9	27.7 | 25.8	26.8

Table 4 shows the estimations of the main and interaction effects, including the standard error, t(9) value, and *p* value. The effects in bold were considered significant (at a 95% confidence level).

Table 4. Main and interaction effects for BSC and SSC.

	BSC				SSC			
	Effect	**Std. Err. Pure Err**	**t(9)**	***p***	**Effect**	**Std. Err. Pure Err**	**t(9)**	***p***
Mean/ Interc.	**26.71**	**0.34**	**77.8939**	**0.0000**	**23.45**	**0.45**	**52.4377**	**0.0000**
Curvatr.	−1.72	2.06	−0.8384	0.4235	**6.51**	**2.68**	**2.4261**	**0.0382**
(1) T (°C)	−0.65	0.69	−0.9477	0.3680	−0.01	0.89	−0.0116	0.9910
(2) t (min)	−0.35	0.69	−0.5103	0.6221	0.20	0.89	0.2213	0.8298
(3) C (mol/L^{-1})	**−13.72**	**0.69**	**−20.0111**	**0.0000**	**−11.97**	**0.89**	**−13.3802**	**0.0000**
1 by 2	−1.3250	0.69	−1.9319	0.0854	−1.01	0.89	−1.1296	0.2879
1 by 3	**2.5000**	**0.69**	**3.6450**	**0.0054**	**2.90**	**0.89**	**3.2490**	**0.0100**
2 by 3	**1.7000**	**0.69**	**2.4786**	**0.0351**	−0.9271	0.89	−1.0364	0.3270
1 × 2 × 3	−1.2750	0.69	−1.8590	0.0960	**−2.09**	**0.89**	**−2.3407**	**0.0440**

The t value is the test statistic from a Student's *t*-test, with the number nine representing the degrees of freedom. The *p* value indicates the probability of obtaining a result as extreme, as observed under the null hypothesis, which typically means no significant effect. A low *p* value (below 0.05 or 0.01) provides strong evidence against the null hypothesis, suggesting that the factor has a significant impact on the dependent variable. This statistical analysis enables inferences to be made about the population from the sample data, determining the reliability of the observed effects [27].

For the BSC, Table 4 indicates that, among the main effects, only the catalyst concentration C demonstrated statistical significance. Both the temperature (T) and constant heating time (t) affected the yield through significant interactions with the potassium carbonate concentration (T × C and t × C). The remaining effects did not exhibit statistical significance within the studied range at the same confidence level.

For the bagasse, the parameter that exhibited the most significant influence and consequently had the highest impact on the bio-oil yield was the catalyst concentration. In the presence of K_2CO_3, there was an average difference of 13.7% in the bio-oil yield, which corresponds to an approximate reduction of 60% in the yield when the catalyst was used. The impact of the catalyst on the yield will be discussed in detail in the next section.

On the other hand, the interaction effects (T × C and t × C), while also relevant, had a comparatively smaller effect than the catalyst concentration. Following Barros Neto et al. [27], a positive interaction effect between two factors indicates that the response variable increases when both factors change in the same direction, meaning they either increase together (move from low to high levels) or remain at low levels together. This implies that the combined effect of these factors on the response is greater than the sum of their individual effects. In other words, the presence of both factors acting in tandem enhances the overall response more significantly than if they were to operate independently. This type of interaction suggests a synergistic relationship, where the combination of factors results in a total effect that is higher than the sum of the individual effects of those factors. This can be observed in various fields, as it indicates that, by optimizing specific conditions, significantly higher results can be achieved.

Since it is already known that the lower level of C (absence of K_2CO_3) favors bio-oil formation, it is thus necessary to keep the temperature at its lowest level (300 °C) so that the effect of T × C positively contributes to the yield. Similarly, a corresponding interpretation applies to the impact of t × C, i.e., a constant heating time of 0 min results in a higher bio-oil yield.

In the context of using sugarcane straw, Table 4 shows that the catalyst concentration also stands out as the most influential parameter, as evidenced by its greater impact on

the bio-oil yield. When K_2CO_3 is employed, the yield decreases by 12% on average. Additionally, it is relevant to note that the synergy effects between the temperature and catalyst concentration T × C, as well as the interaction effect among all three T × t × C factors, also showed statistical significance regarding the yield obtained from sugarcane straw.

The curvature test shows that there is significant curvature in the data, so that a linear model is not suitable for adequately representing our results. However, as there are also significant interaction effects, a clearer representation of the impact of these effects on the bio-oil yield is provided in Figure 2, which presents a cube plot where each axis represents a variable (T, t, or C).

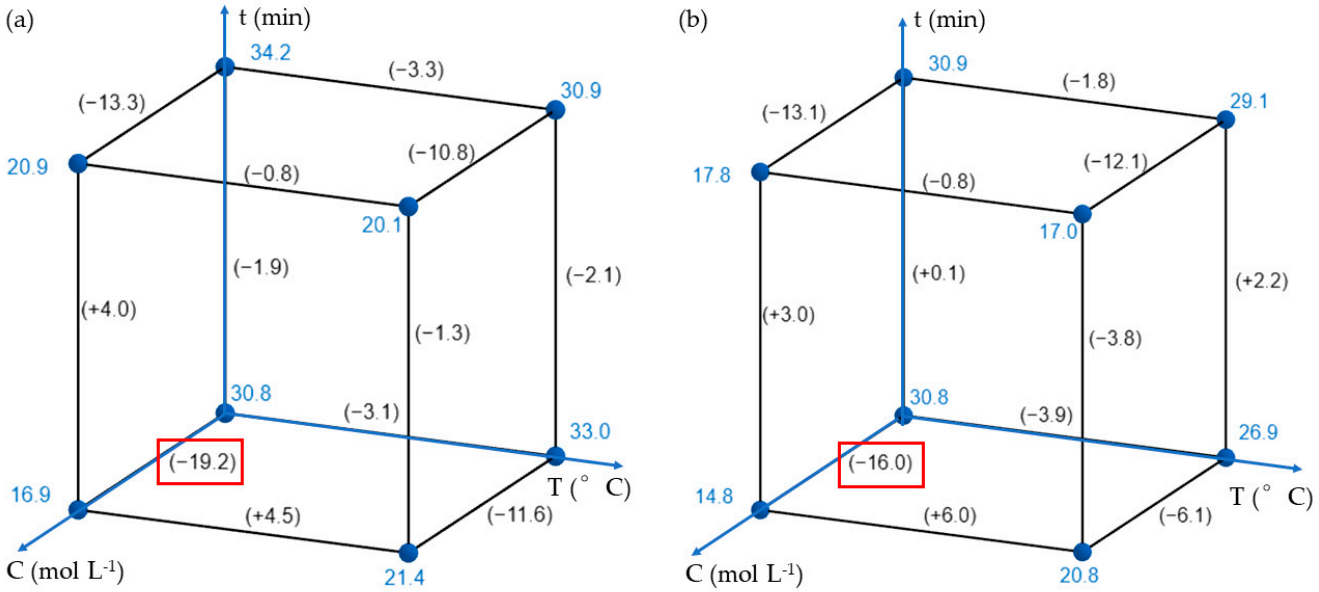

Figure 2. Cube plot illustrating the impact of effects on bio-oil yield for (**a**) BSC and (**b**) SSC experiments. In blue, the mean response under each experimental condition. In parenthesis, estimated effects.

For bagasse, as illustrated in Figure 2a, the combination of experimental parameters that resulted in the maximum bio-oil production consisted of maintaining the temperature constant at 300 °C, with a **c**onstant heating time of 0 min, and without the inclusion of a catalyst, resulting in an average bio-oil yield of 36.2% by mass. The interaction effects of T × t and T × C can also be visualized. For example, depending on the levels of the other variables, the effect of raising the temperature can be positive (with K_2CO_3 and 0 min), negative (without K_2CO_3, 0 or 30 min), or without significant effect (with K_2CO_3 and 30 min). The effect of using K_2CO_3 is more pronounced (with a 19% decrease in the yield) when the temperature and **c**onstant heating time are at the lowest levels (0 min and 300 °C). This suggests that the inhibition of desirable reactions may be occurring. K_2CO_3 might inhibit reactions that favor bio-oil formation under low-temperature and short **c**onstant heating time conditions. Additionally, the presence of the catalyst may promote an increase in water-soluble compounds in the aqueous phase.

For straw, Figure 2b shows that the combination of experimental parameters that resulted in the maximum bio-oil production was the maintenance of the temperature at 300 °C, without K_2CO_3. The time is not significant, resulting in an average bio-oil yield of 30.9% (0 min) or 30.8% (30 min). As a negligible impact of time on the bio-oil yield ±0.05%) was observed, using a 0 min **c**onstant heating time is more advantageous. Therefore, for straw, the optimal condition was considered to be 300 °C, 0 min, and the absence of the catalyst.

The two and three factors' interaction effects (T × C and T × t × C) can also be visualized and interpreted. Similar to the results seen for the bagasse, depending on the

levels of the other variables, the effects of raising the temperature and time can be positive, negative, or without significance. The effect of using K_2CO_3 is more pronounced (a decrease of 16% in the yield) when the temperature and time are within the low levels (0 min and 300 °C). On the other hand, when the temperature is 350 °C, the decrease in the yield is only 6%. This occurs because K_2CO_3 can catalyze dehydration and decarboxylation reactions at lower temperatures, resulting in greater gas formation and lower bio-oil yields. At higher temperatures, these reactions may be less favored or offset by other reactions that increase the bio-oil yield.

3.1.2. Effect of Process Parameters on Product Yields

Each biomass was subjected to 18 experiments in which the nine conditions of the experimental design were carried out in duplicate. Figures 3 and 4 illustrate the results obtained regarding the mean yields, under each experimental condition, for the four products in the HTL experiments with BSC and SSC.

An analysis of Figure 3 indicates two distinct patterns in the yields of the product fractions, and these are related to the presence or absence of a catalyst in the experiments. While bio-oil production was favored in the experiments without a catalyst, as discussed in the previous section, the aqueous fraction was higher in the experiments conducted with a catalyst.

Figure 3 also reveals that the fraction of soluble organic compounds forming the aqueous phase was the largest fraction produced in all experiments, reaching 42.7% in the experiment without the catalyst (BSC350-30) and 71.2% in the experiment with the catalyst (BSC300-0C). The experiment that exhibited the highest bio-oil yield produced approximately the same fractions of bio-oil and aqueous phase, reaching a 36.9% yield of aqueous phase.

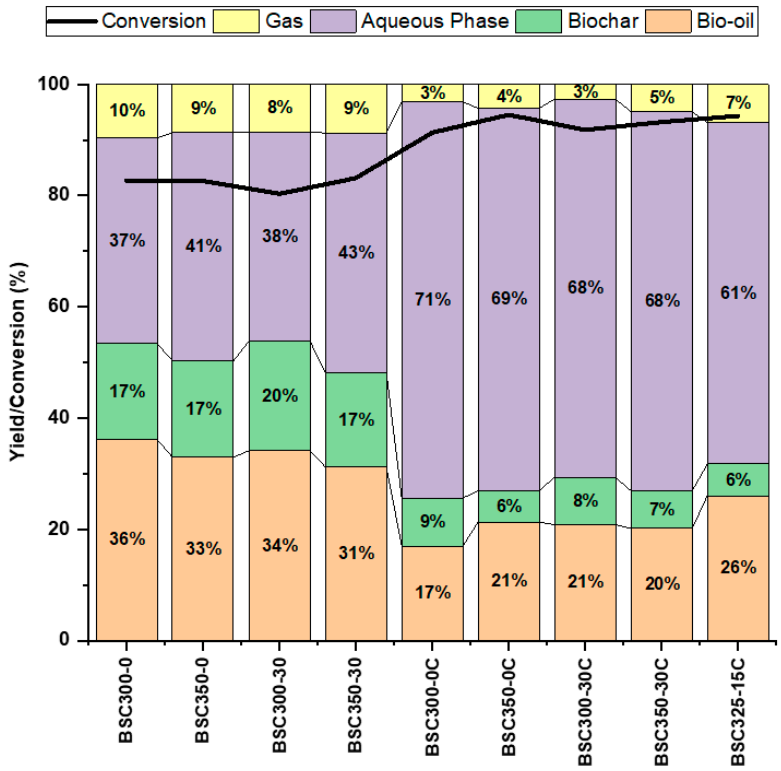

Figure 3. Average yield of products and biomass conversion for BSC.

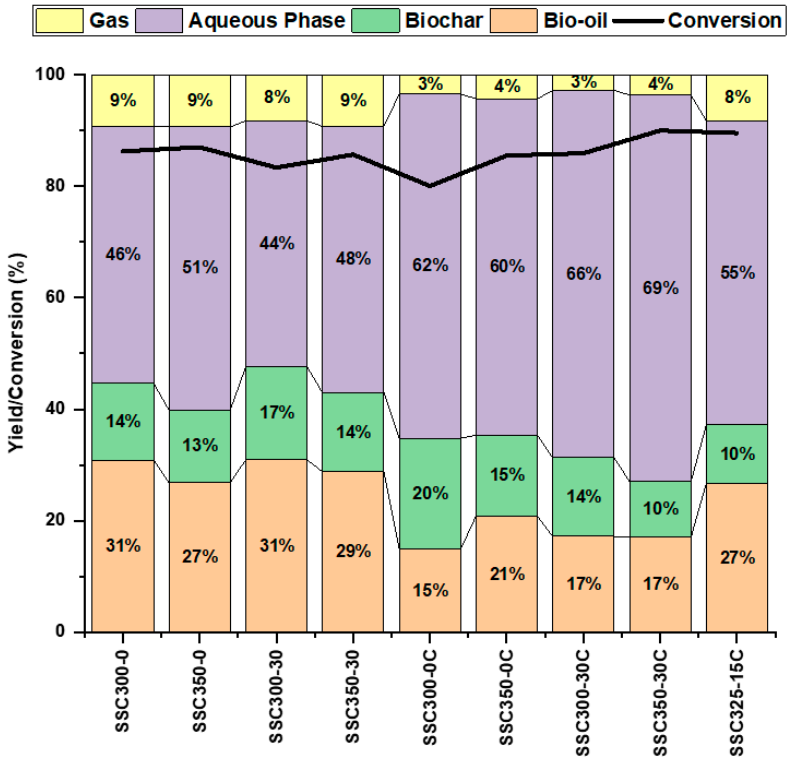

Figure 4. Average yield of products and biomass conversion for SSC.

These results also indicate an increase in conversion compared to the non-catalytic experiments, attributed in particular to the predominance of the aqueous phase in the catalytic experiments. In line with the implication of these findings, Jindal and Jha [26] reported the role of homogeneous alkaline catalysts in biomass depolymerization and the inhibition of repolymerization. On the other hand, Gan and Yuan [28] drew attention to the significant insight that an excessive quantity of these catalysts may lead to an overly extensive depolymerization of biomass or the degradation of already-formed bio-oil compounds. This could culminate in the production of gases and low-molecular-weight compounds that are soluble in water.

Relevant to the two behavior patterns, there was a higher conversion in the experiments involving the use of a catalyst. This conversion, however, did not necessarily result in biomass converted into bio-oil but rather was more likely to result in conversion into aqueous phase. In a study conducted by Beims et al. [29], the authors mention this behavior as a disadvantage of the hydrothermal liquefaction of biomass. They explain that the liquid organic products generated are distributed between bio-oil and aqueous phase. A commonly used approach is to extract these organic compounds using a suitable solvent [26,30,31].

Singh et al. [25] reported a bio-oil yield of 25% and an aqueous phase yield of 49% when sugarcane bagasse was processed without a catalyst. Comparable outcomes were observed by Mathanker et al. [22] in their study on the liquefaction of lignocellulosic biomass (corn stalk), where they achieved a bio-oil yield of 29.3% and a yield of 42% for the water-soluble organic compounds formed during the reactions.

The results of the yields of the four product fractions in the experiments with sugarcane straw shown in Figure 4 show a certain similarity to the results already mentioned for sugarcane bagasse.

Regarding the experiments with SSC, compared to BSC, a slight decrease in the conversion and yield values of the bio-oil fraction was observed, along with a slight increase in the biochar fraction for the experiments involving a catalyst. The gas and aqueous phase fractions, however, were within the same ranges. The lignocellulosic compositions of these

two feedstocks (as shown in Table 1) suggest possible reasons for this similarity in results; the level of impurities (extractives and ash) in the straw may account for these differences. These impurities were not removed because the study aimed to replicate conditions of real-world scenarios, where industrial/agricultural residues, as received, would include such impurities, as closely as possible.

Using water as a solvent, the decomposition of the main components of lignocellulosic materials follows a specific order. Hemicellulose decomposes first, usually from 200 °C to 300 °C, followed by cellulose, which decomposes between 300 and 400 °C. Lignin decomposes more slowly and over a wider temperature range, between 250 and 500 °C [29]. Taking this into account, and comparing the bio-oil yields of the sugarcane bagasse with those of the sugarcane straw, the lower bio-oil production observed in the experiments with sugarcane straw can possibly be attributed to the straw's lower cellulose and lignin contents. Moreover, sugarcane straw contains higher levels of extractives and ash, which introduce additional impurities (Table 1).

3.2. Spectral Attributes

The raw spectra acquired from the bio-oils (Figure 5a,b) presented some effects of radiation scattering, a typical condition for infrared spectra that is commonly associated with the acquisition process. Regarding the spectral profiles, some bands are highlighted, such as those around 1700 cm^{-1}, 3300 cm^{-1}, 3000–2800 cm^{-1} and, 1200 cm^{-1}. These regions are associated with the C=O, O–H, C–H (aliphatic compounds) and C-O stretching vibrations. All of these groups may be associated with oxygenated compounds, such as carboxylic acids, phenols, aldehydes, esters, alcohols, ethers, and ketones. These classes of compounds have been commonly reported in the literature as being observed in hydrothermal liquefaction bio-oil compositions when lignocellulosic biomasses are used as feedstock [1,21,23,32].

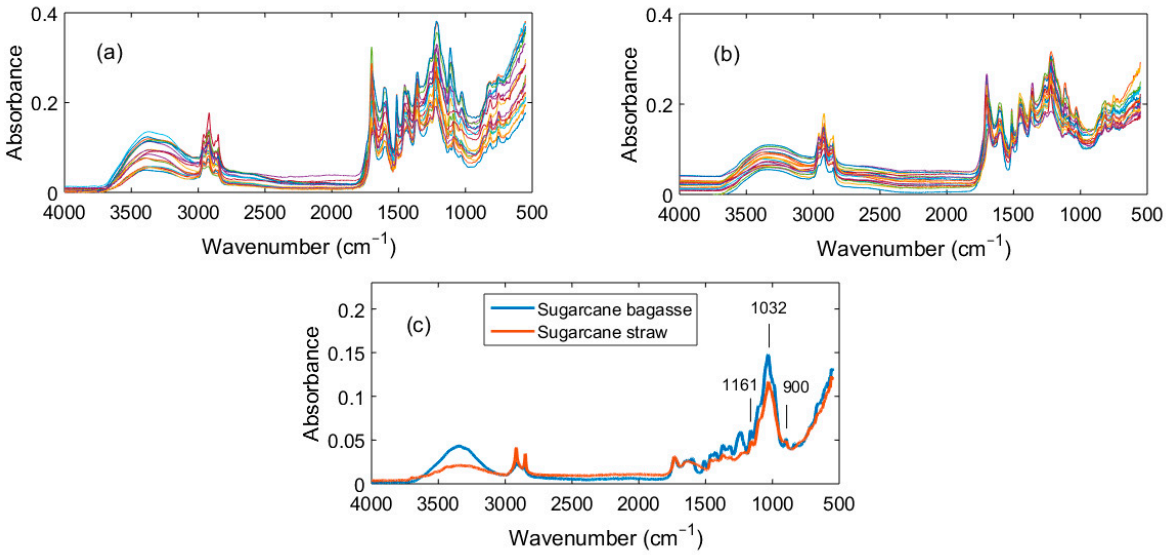

Figure 5. FTIR spectra from (**a**) bio-oils produced from sugarcane bagasse; (**b**) bio-oils produced from sugarcane straw; and (**c**) raw biomasses.

In addition, according to Figure 5a,b, regardless of the kind of biomass employed in the thermochemical conversion, the MIR spectra of the bio-oils exhibit the absence of bands at approximately 1000 cm^{-1}. This absence can be indicative of a structural break of the main compounds present in the biomasses that were used: cellulose, hemicellulose, and lignin. These three bands are highlighted in the corresponding feedstock MIR spectra (Figure 5c).

In Figure 5c, at 1032 cm^{-1}, a C–O–C pyranose ring (antisymmetric in phase ring) stretching vibration is noticeable. This band has the most intense spectral signal due to its

presence in two of the majority compounds (cellulose and hemicellulose) in both biomasses. The C–C ring vibration is about 1161 cm^{-1}; in addition, a small shoulder can be seen at 1105 cm^{-1} that is related to the C–O–C glycosidic ether band, which is also associated with the polysaccharides cellulose and hemicellulose. Furthermore, another characteristic spectral signal is observed at 900 cm^{-1}; this is associated with the β-glycosidic linkages between glucose units in cellulose, and is also present in the hemicellulose chain [33].

3.3. Pre-Processing and Exploratory Analysis

In order to obtain more information about the bio-oil samples from the MIR spectra data, a principal component analysis (PCA) was performed. First, a preprocessing step was carried out to minimize some base line shifts present in the spectra (Figure 6a,b). The first-order derivative (second-order polynomial and window size of 25 points) provided the best results in terms of correcting the physical deviations and was also able to highlight the differences between the bio-oils obtained from sugarcane bagasse and straw, as described in Figure 6a.

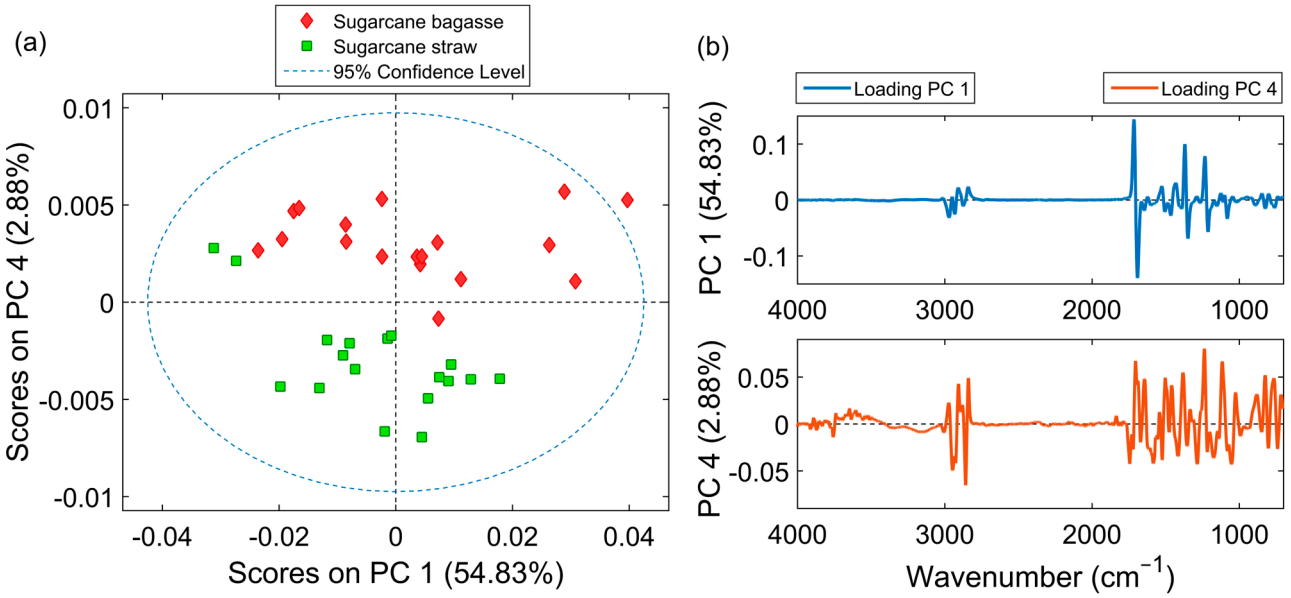

Figure 6. Principal components analysis of bio-oils produced from sugarcane bagasse and straw: (**a**) scores and (**b**) loadings plots for PC1 and PC4. Dataset preprocessed with first derivative with a window size of 25 and mean center.

The PCA model shows that the first four principal components (PCs) described 93.1% of the variations in the data. An analysis of the PCA score plots shows only two clusters along PC4 (Figure 6a), which is the main PC responsible for clarifying the differences among the bio-oil samples produced by the different biomasses.

The corresponding loading plots are shown in Figure 6b. In particular, in the latter, the absorptions from 3000 to 2800 cm^{-1} (C-H stretching) are associated with the presence of aliphatic compounds, whose region seems to influence the separation observed in the PC4 score plot. Since an in-depth interpretation is allowed by the intrinsic effect of the derivative preprocessing strategy, it is still possible to observe the contribution of the entire fingerprint region in PC4 to the bio-oils' separation. Within this region, absorptions in the regions such as 1700 cm^{-1} and, 1200–1000 cm^{-1} are related to oxygenated compounds, especially those with carbonyl (C=O) and C-O groups. This is consistent with the biomass sources used, which consist mainly of oligosaccharides such as cellulose, hemicellulose, and lignin, which are oxygenated polymers [22,32,33].

3.4. Chemical Composition of Bio-Oil by GC-MS

The bio-oil samples obtained with the highest yields were characterized by GC-MS and a detailed composition analysis is presented in Table 5. The GC-MS analysis detected a number of compounds using the BSC library; however, Table 5 only lists compounds with an area fraction greater than 1%. Thus, 14 (BSC300-0) and 13 components (BSC300-0C) were detected in the bio-oils derived from bagasse, respectively, whereas, in the bio-oils from straw, 20 (SSC300-0) and 23 components (SSC300-0C) were identified [10,19,24,34–39].

Table 5. Chemical composition as identified by GC-MS analysis of BCS and SSC bio-oils *.

S. n.	Name	t_R (min)	Chemical Class	Molecular Formula	Relative Area (%)			
					BSC300-0	BCS300-0C	SSC300-0	SCS300-0C
1.	2,6-Dimethyl pyridine	12.296	Nitrogenous	C_7H_9N	n.d.	2.25	n.d.	n.d.
2.	Acetoacetic acid, 1-thio-	12.451	Thiocompounds	$C_8H_{14}O_2S$	1.33	n.d.	n.d.	n.d.
3.	Tetrahydro-2-methylfuran	12.583	Furan	$C_5H_{10}O$	n.d.	1.12	n.d.	n.d.
4.	Oxirane, (1-methylbutyl)-	13.642	Oxygenated	$C_7H_{14}O$	n.d.	n.d.	4.74	2.36
5.	n-Octenol	13.656	Oxygenated	$C_8H_{16}O$	n.d.	n.d.	4.41	6.58
6.	2-(Pentyloxy)ethanol	13.775	Oxygenated	$C_7H_{16}O$	n.d.	n.d.	26.76	13.32
7.	3 Methyl-Propanol	13.872	Oxygenated	$C_4H_{10}O$	40.46	59.02	n.d.	n.d.
8.	Phenol	14.879	Oxygenated	C_6H_6O	n.d.	3.59	1.36	5.22
9.	Ethylamine	14.884	Nitrogenous	$C_2H_5NH_2$	1.59	2.21	3.04	2.86
10.	Ethane-1,2-diol	15.761	Oxygenated	$C_2H_6O_2$	2.03	1.84	n.d.	n.d.
11.	2-Methoxyphenol	16.072	Oxygenated	$C_7H_8O_2$	n.d.	3.56	1.07	4.77
12.	n-Propenol	16.352	Oxygenated	C_3H_8O	6.97	2.71	3.50	3.18
13.	2-Hydroxypropanoic acid	16.359	Oxygenated	$C_3H_6O_3$	3.39	n.d.	4.83	4.36
14.	Methyl-2-hydroxypropanoate	16.465	Oxygenated	$C_4H_8O_3$	5.75	n.d.	n.d.	n.d.
15.	Ethanol	17.249	Oxygenated	C_2H_5O	n.d.	n.d.	1.12	1.61
16.	2-Hydroxybutyric acid	19.158	Oxygenated	$C_4H_8O_3$	n.d.	n.d.	n.d.	2.97
17.	Hexadecanoic acid, 2,3-dihydroxypropyl ester	19.705	Oxygenated	$C_{19}H_{38}O_4$	n.d.	n.d.	1.22	2.64
18.	2,3-Dihydroxypropanoic acid	19.858	Oxygenated	$C_3H_6O_4$	1.42	n.d.	2.02	n.d.
19.	Methanol	19.947	Oxygenated	CH_3OH	n.d.	1.18	n.d.	n.d.
20.	4-Hydroxy-3-methoxybenzaldehyde	21.849	Oxygenated	$C_8H_8O_3$	n.d.	1.82	1.22	2.55
21.	p-Nitrophenol	23.284	Nitrogenous	$C_6H_5NO_3$	n.d.	3.40	n.d.	2.51
22.	2-Methoxyphenol	23.432	Oxygenated	$C_7H_8O_2$	n.d.	1.08	n.d.	4.77
23.	3,7,11,15,18-Pentaoxa-2,19-disilaeicosane, 2,2,19,19-tetramethyl	24.045	Oxygenated	$C_{17}H_{40}O_5Si_2$	n.d.	n.d.	1.80	n.d.
24.	3,5-Dimethylphenol	26.281	Oxygenated	$C_8H_{10}O$	1.16	1.55	2.52	2.43
25.	Propane-1,2,3-triol	27.448	Oxygenated	$C_3H_8O_3$	n.d.	n.d.	13.06	10.09
26.	Propyl stearate	29.310	Oxygenated	$C_{21}H_{42}O_2$	n.d.	n.d.	3.34	1.67

Table 5. *Cont.*

S. n.	Name	t_R (min)	Chemical Class	Molecular Formula	Relative Area (%)			
					BSC300-0	BCS300-0C	SSC300-0	SCS300-0C
27.	4-methyl-phenol	32.407	Oxygenated	C_7H_8O	n.d.	n.d.	n.d.	1.58
28.	Oleic acid	37.621	Oxygenated	$C_{18}H_{34}O_2$	n.d.	n.d.	n.d.	1.36
29.	Pentanoic acid	51.248	Oxygenated	$C_5H_{10}O_2$	n.d.	n.d.	n.d.	1.31
30.	9,12-Octadecadienoic acid (Z,Z)-, methyl ester	52.847	Oxygenated	$C_{19}H_{34}O_2$	1.29	n.d.	n.d.	n.d.
31.	9-Octadecenoic acid (Z)-, methyl ester	52.969	Oxygenated	$C_{19}H_{36}O_2$	1.08	n.d.	n.d.	n.d.
32.	Hexadecanoic acid	55.349	Oxygenated	$C_{16}H_{32}O_2$	n.d.	n.d.	1.22	2.64
33.	Octadecanoic acid	55.868	Oxygenated	$C_{18}H_{36}O_2$	n.d.	n.d.	n.d.	1.20
34.	Tetrapentacontane	56.517	Hydrocarbon	$C_{54}H_{110}$	n.d.	n.d.	2.74	n.d.
35.	Tetracontane	56.662	Hydrocarbon	$C_{40}H_{82}$	8.99	n.d.	1.33	n.d.
36.	4-Hydroxybenzaldehyde	62.820	Oxygenated	$C_7H_6O_2$	n.d.	n.d.	n.d.	n.d.
37.	Butanedioic acid	66.594	Oxygenated	$C_4H_6O_4$	n.d.	n.d.	n.d.	1.15
38.	Hexatriacontane	66.814	Hydrocarbon	$C_{36}H_{74}$	n.d.	n.d.	7.61	n.d.
39.	Dotriacontane	66.881	Hydrocarbon	$C_{32}H_{66}$	9.25	n.d.	n.d.	n.d.
40.	Nonacosane	68.993	Hydrocarbon	$C_{29}H_{60}$	5.05	n.d.	n.d.	n.d.

* produced from HTL at 300 °C and 0 min for constant heating time, with or without the presence of catalysts; n.d = not detected.

These results indicate that bio-oils derived from straw exhibit a greater diversity of compounds compared to those from bagasse. In short, the three major compounds are: 3-methyl-propanol (59.0%) in BSC300-0C, and 2-(pentyloxy) ethanol (26.8%) and propane-1,2,3-triol (13.1%) in SSC300-0. These compounds are derived from the breakdown of cellulose and hemicellulose, which are more abundant components than lignin in the composition of lignocellulosic biomass [10,31,32].

Table 5 also shows that the chemical compositions of bio-oils consist primarily of aliphatic and aromatic compounds containing oxygen, nitrogen, and sulfur components, which are classified into various chemical classes [19,22,33,34].

Other bio-oil components have also been organized into chemical classes, such as oxygenated compounds (alcohols, phenols, esters, carboxylic acids, ketones, aldehydes, lactones), nitrogen compounds (amines and pyridines), hydrocarbons, furans, and sulfur compounds (thiocompounds), as shown in Figure 7.

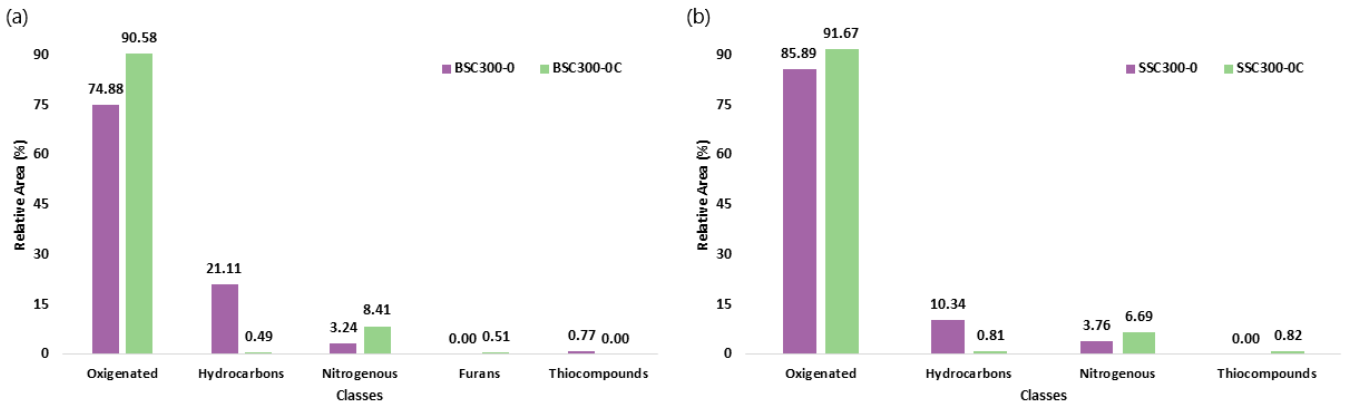

Figure 7. Chemical classes of GC-MS results of BSC (**a**) and SSC (**b**) bio-oils produced from HTL at 300 °C and 0 min of constant heating time, with or without the presence of catalysts.

The bio-oils from both BSC and SSC presented a high content of oxygenated compounds (Figure 7), composed mainly of alcohols, esters, phenols, carboxylic acids, aldehydes, and ethers. In the BSC bio-oils, the presence of the catalyst can be seen to increase the content of oxygenated compounds, especially those in the classes of phenols, carboxylic acids, and esters. The same behavior was found in the SSC straw bio-oils (except for the furan class).

In general, the SSC bio-oils presented a higher content of oxygenated compounds compared to the BSC bio-oils, regardless of whether or not a catalyst was used (Figure 7). Moreover, the highest content was found in the presence of the catalyst for each: BSC bio-oil (90.6%) and SSC bio-oil (91.7%). This can be explained by the effect of the catalyst, which can increase the conversion of the biomass decomposition, which in turn directly influences the content of oxygenated compounds in the bio-oils, as also reported by Cao et al. [34] and Madsen et al. [35].

Degradation of the lignin present in lignocellulosic biomass produces phenolic compounds, as reported by various studies that have converted lignocellulosic biomass into bio-oils [34–39]. Lignin breakdown can generate phenol, *p*-cresol (4-methyl-phenol), and guaiacol (2-methoxyphenol), which have been detected with relative area fractions ranging from 1.0% to 3.6%. Lignin is the most challenging component to degrade within biomass; the use of a catalyst has been observed to significantly enhance its degradation efficiency. Thus, the use of a homogeneous alkaline catalyst reduces the stability of the C-C bonds (5-5, β-5, β-β′, β-1) in the lignin structure, facilitating its degradation, which can explain the increase in the amounts of phenolic compounds in the bio-oils produced with the catalyst [34,40].

A preliminary analysis of the potential of a bio-oil to become a biofuel can be carried out by analyzing the content of hydrocarbons in the bio-oil. Figure 7 shows that the highest hydrocarbon content was found without the use of catalyst, with values of 21.1% and 10.3% for the BSC and SSC bio-oils, respectively. For example, dotriacontane (9.2%) and tetracontane (9%) were detected in BSC300-0, and hexatriacontane (7.6%) was detected in SSC300-0. The majority of the hydrocarbons in bio-oils come from the reaction's preference for breaking down long-chain aliphatic oxygenated compounds [41]. The use of the catalyst in the production process of both bio-oils using HTL was not considered to contribute to the formation of hydrocarbon compounds.

4. Conclusions

This study demonstrated that the hydrothermal liquefaction of sugarcane bagasse and straw can effectively produce bio-oil under subcritical conditions using water as a solvent. The key findings indicate that optimal bio-oil yields were achieved at 300 °C, without the use of a catalyst, and with minimum constant heating times. The analysis revealed a complex relationship between the factors influencing bio-oil production, with notable differences in yields between sugarcane bagasse and straw. Importantly, the presence of a catalyst was found to significantly reduce bio-oil yields while promoting the formation of water-soluble compounds. Additionally, spectral analysis showed that the bio-oils contained a high proportion of oxygenated compounds, indicative of the structural breakdown of biomass. Furthermore, bio-oil spectra exhibited the absence of bands related to major biomass components (cellulose, hemicellulose, and lignin), indicative of structural breakdown. PCA model results demonstrated the clear differentiation of bio-oil samples from different biomasses, with aliphatic and oxygenated compounds playing significant roles in the cluster formation. GC-MS analysis revealed a high content of oxygenated compounds in both bio-oils, predominantly alcohols, esters, phenols, carboxylic acids, aldehydes, and ethers. The presence of the catalyst significantly increased the contents of these compounds in both the BSC and SSC bio-oils, while also promoting greater lignin decomposition and phenolic compound formation, and reduced the production of hydrocarbon.

These findings provide valuable insights for optimizing lignocellulosic biomass conversion processes, particularly regarding product fraction yields and K_2CO_3 catalyst use, contributing to the development of sustainable biofuel production strategies.

Author Contributions: Conceptualization: L.D., D.A.S. and R.S.S.; methodology: R.S.S., R.A.d.S.J., F.M.d.A. and R.M.d.N.; software: R.S.S. and F.M.d.A.; validation: R.S.S., M.F.P. and F.M.d.A.; formal analysis: L.D.; investigation: R.S.S., R.A.d.S.J., P.N.A.N. and F.M.d.A.; resources: D.A.S.; data curation: R.S.S., F.M.d.A. and R.M.d.N.; writing—original draft preparation: R.S.S., F.M.d.A. and R.M.d.N.; writing—review and editing: L.D. and L.S.; visualization: M.F.P., L.S. and J.M.S.; supervision: L.D. and J.M.S.; project administration: D.A.S.; funding acquisition: D.A.S. and L.S. All authors have read and agreed to the published version of the manuscript.

Funding: This research was funded by FACEPE (H2020 and BioValue Project APQ-0074-3.06/19), IBPG 0255-1.06/20, Brazil's Coordination for the Improvement of Higher Education Personnel (CAPES), CAPES/DS (project 88882.379823/2019-01) and CNPq (401342/2022-0).

Data Availability Statement: Data is contained within the article.

Acknowledgments: The authors acknowledge the support by FACEPE, PETROBRAS, KLABIN, SUZANO, EMBRAER, and CNPEM/LNBR within the scope of the BioValue project.

Conflicts of Interest: The authors declare no conflicts of interest.

References

1. Forero, J.A.J.; Tran, T.H.T.; Tana, T.; Baker, A.; Beltramini, J.; Doherty, W.O.S.; Moghaddam, L. Hydrothermal Liquefaction of Sugarcane Bagasse to Bio-Oils: Effect of Liquefaction Solvents on Bio-Oil Stability. *Fuel* **2022**, *312*, 122793. [CrossRef]
2. Hussin, F.; Hazani, N.N.; Khalil, M.; Aroua, M.K. Environmental Life Cycle Assessment of Biomass Conversion Using Hydrothermal Technology: A review. *Fuel Process. Technol.* **2023**, *246*, 107747. [CrossRef]
3. Marx, S.; Laubscher, A.N.E.; Bunt, J.R.; Venter, R.J.; Uwaoma, R.C.; Strydom, C.A. Evaluation of Sugar Cane Bagasse Hydrothermal Liquefaction Products for Co-Gasification with Coal as Green Coal Pellet Production. *Bioresour. Technol. Rep.* **2023**, *22*, 101503. [CrossRef]
4. Negrão, D.R.; Grandis, A.; Buckeridge, M.S.; Rocha, G.J.M.; Leal, M.R.L.V.; Driemeier, C. Inorganics in Sugarcane Bagasse and Straw and Their Impacts for Bioenergy and Biorefining: A review. *Renew. Sustain. Energy Rev.* **2021**, *148*, 111268. [CrossRef]
5. Kumar, A.; Jamro, I.A.; Rong, H.; Kumari, L.; Laghari, A.A.; Cui, B.; Aborisade, M.A.; Oba, B.T.; Nkinahamira, F.; Ndagijimana, P.; et al. Assessing Bioenergy Prospects of Algal Biomass and Yard Waste Using an Integrated Hydrothermal Carbonization and Pyrolysis (HTC–PY): A Detailed Emission–to–Ash Characterization via Diverse Hyphenated Analytical Techniques and Modelling Strategies. *Chem. Eng. J.* **2024**, *492*, 152335. [CrossRef]
6. Qiu, B.; Shi, J.; Hu, W.; Gao, J.; Li, S.; Chu, H. Construction of Hydrothermal Liquefaction System for Efficient Production of Biomass-derived Furfural: Solvents, Catalysts and Mechanisms. *Fuel* **2023**, *354*, 129278. [CrossRef]
7. Santos, J.C.M. Produção de Combustíveis Alternativos a Partir de Resíduos de Biomassa Verde por Conversão Hidrotérmica. Master's Thesis, Universidade de Lisboa, Lisboa, Portugal, 2016. Available online: http://hdl.handle.net/10451/26170 (accessed on 4 June 2024).
8. Kruse, A.; Dahmen, N. Hydrothermal Biomass Conversion: Quo vadis? *J. Supercrit. Fluids* **2018**, *134*, 114–123. [CrossRef]
9. Akhtar, J.; Kuang, S.K.; Amin, N.A.S. Liquefaction of Empty Palm Fruit Bunch (EPFB) in Alkaline Hot Compressed Water. *Renew. Energy* **2010**, *35*, 1220–1227. [CrossRef]
10. Nunes, V.O.; Fraga, A.C.; Silva, R.V.S.; Pontes, N.S.; Pinho, A.R.; Sousa-Aguiar, E.F.; Azevedo, D.A. Chemical Characterisation of Sugarcane Bagasse Bio-Oils from Hydrothermal Liquefaction: Effect of Reaction Conditions on Products Distribution and Composition. *J. Environ. Chem. Eng.* **2021**, *9*, 106513. [CrossRef]
11. Castello, D.; Pedersen, T.H.; Rosendahl, L.A. Continuous Hydrothermal Liquefaction of Biomass: A Critical Review. *Energies* **2018**, *11*, 3165. [CrossRef]
12. Hietala, D. Advancing Empirical Models for the Hydrothermal Liquefaction of Microalgae. Ph.D. Thesis, University of Michigan, Ann Arbor, MI, USA, 2018. Available online: https://deepblue.lib.umich.edu/handle/2027.42/145873 (accessed on 10 July 2024).
13. Zhang, S.; Yang, X.; Zhang, H.; Chu, C.; Zheng, K.; Ju, M.; Liu, L. Liquefaction of Biomass and Upgrading of Bio-Oil: A Review. *Molecules* **2019**, *24*, 2250. [CrossRef]
14. Biller, P.; Ross, A.B. Potential Yields and Properties of Oil from the Hydrothermal Liquefaction of Microalgae with Different Biochemical Content. *Bioresour. Technol.* **2011**, *102*, 215–225. [CrossRef] [PubMed]
15. Li, Y.; Zhu, C.; Jiang, J.; Yang, Z.; Feng, W.; Li, L.; Guo, Y.; Hu, J. Catalytic Hydrothermal Liquefaction of *Gracilaria corticata* Macroalgae: Effects of Process Parameter on Bio-Oil Up-gradation. *Bioresour. Technol.* **2021**, *319*, 124163. [CrossRef] [PubMed]
16. Yin, S.; Dolan, R.; Harris, M.; Tan, Z. Subcritical Hydrothermal Liquefaction of Cattle Manure to Bio-Oil: Effects of Conversion Parameters on Bio-Oil Yield and Characterization of Bio-Oil. *Bioresour. Technol.* **2010**, *101*, 3657–3664. [CrossRef] [PubMed]

17. Yan, X.; Ma, J.; Wang, W.; Zhao, Y.; Zhou, J. The Effect of Different Catalysts and Process Parameters on the Chemical Content of Bio-oils from Hydrothermal Liquefaction of Sugarcane Bagasse. *Bioresources* **2017**, *13*, 997–1018. [CrossRef]
18. Brand, S.; Hardi, F.; Kim, J.; Suh, D.J. Effect of Heating Rate on Biomass Liquefaction: Differences Between Subcritical Water and Supercritical Ethanol. *Energy* **2014**, *68*, 420–427. [CrossRef]
19. Long, J.; Li, Y.; Zhang, X.; Tang, L.; Song, C.; Wang, F. Comparative Investigation on Hydrothermal and Alkali Catalytic Liquefaction of Bagasse: Process Efficiency and Product Properties. *Fuel* **2016**, *186*, 685–693. [CrossRef]
20. Brand, S.; Susanti, R.F.; Kim, S.K.; Lee, H.S.; Kim, J.; Sang, B.I. Supercritical Ethanol as an Enhanced Medium for Lignocellulosic Biomass Liquefaction: Influence of Physical Process Parameters. *Energy* **2013**, *59*, 173–182. [CrossRef]
21. de Caprariis, B.; de Filippis, P.; Petrullo, A.; Scarsella, M. Hydrothermal Liquefaction of Biomass: Influence of Temperature and Biomass Composition on the Bio-Oil Production. *Fuel* **2017**, *208*, 618–625. [CrossRef]
22. Mathanker, A.; Pudasainee, D.; Kumar, A.; Gupta, R. Hydrothermal Liquefaction of Lignocellulosic Biomass Feedstock to Produce Biofuels: Parametric Study and Products Characterization. *Fuel* **2020**, *271*, 117534. [CrossRef]
23. Toor, S.S.; Reddy, H.; Deng, S.; Hoffmann, J.; Spangsmark, D.; Madsen, L.B.; Holm-Nielsen, J.B.; Rosendahl, L.A. Hydrothermal Liquefaction of *Spirulina* and *Nannochloropsis salina* Under Subcritical and Supercritical Water Conditions. *Bioresour. Technol.* **2013**, *131*, 413–419. [CrossRef] [PubMed]
24. Durak, H.; Genel, S. Catalytic Hydrothermal Liquefaction of *Lactuca scariola* with a Heterogeneous Catalyst: The Investigation of Temperature, Reaction Time and Synergistic Effect of Catalysts. *Bioresour. Technol.* **2020**, *309*, 123375. [CrossRef]
25. Singh, R.; Prakash, A.; Balagurumurthy, B.; Singh, R.; Saran, S.; Bhaskar, T. Hydrothermal Liquefaction of Agricultural and Forest Biomass Residue: Comparative Study. *J. Mater. Cycles Waste Manag.* **2015**, *17*, 442–452. [CrossRef]
26. Jindal, M.K.; Jha, M.K. Catalytic Hydrothermal Liquefaction of Waste Furniture Sawdust to Bio-Oil. *Indian Chem. Eng.* **2016**, *58*, 157–171. [CrossRef]
27. Barros Neto, B.; Scarminio, I.S.; Bruns, R.E. *Como Fazer Experimentos: Pesquisa e Desenvolvimento na Ciência e na Indústria*, 4th ed.; Bookman: Porto Alegre, Brazil, 2010.
28. Gan, J.; Yuan, W. Operating Condition Optimization of Corncob Hydrothermal Conversion for Bio-Oil Production. *Appl. Energy* **2013**, *103*, 350–357. [CrossRef]
29. Beims, R.F.; Hu, Y.; Shui, H.; Xu, C. Hydrothermal Liquefaction of Biomass to Fuels and Value-Added Chemicals: Products Applications and Challenges to Develop Large-Scale Operations. *Biomass Bioenergy* **2020**, *135*, 105510. [CrossRef]
30. Govindasamy, G.; Sharma, R.; Subramanian, S. Effect of Composition of Iron-Cobalt Oxide Catalyst and Process Parameters on the Hydrothermal Liquefaction of Sugarcane Bagasse. *Bull. Chem. React. Eng. Catal.* **2020**, *15*, 186–198. [CrossRef]
31. Kaur, R.; Biswas, B.; Kumar, J.; Jha, M.K.; Bhaskar, T. Catalytic Hydrothermal Liquefaction of Castor Residue to Bio-Oil: Effect of Alkali Catalysts and Optimization Study. *Ind. Crops Prod.* **2020**, *149*, 112359. [CrossRef]
32. Candido, R.G.; Mori, N.R.; Gonçalves, A.R. Sugarcane Straw as Feedstock for 2G Ethanol: Evaluation of Pretreatments and Enzymatic Hydrolysis. *Ind. Crops Prod.* **2019**, *142*, 111845. [CrossRef]
33. Canettieri, E.V.; da Silva, V.P.; Neto, T.G.S.; Hernández-Pérez, A.F.; da Silva, D.D.V.; Dussán, K.J.; Felipe, M.G.A.; de Carvalho, J.A., Jr. Physicochemical and Thermal Characteristics of Sugarcane Straw and its Cellulignin. *J. Braz. Soc. Mech. Sci. Eng.* **2018**, *40*, 416. [CrossRef]
34. Cao, L.; Luo, G.; Zhang, S.; Chen, J. Bio-Oil Production from Eight Selected Green Landscaping Wastes through Hydrothermal Liquefaction. *RSC Adv.* **2016**, *6*, 15260–15270. [CrossRef]
35. Madsen, R.B.; Jensen, M.M.; Glasius, M. Qualitative Characterization of Solid Residue from Hydrothermal Liquefaction of Biomass Using Thermochemolysis and Stepwise Pyrolysis-Gas Chromatography-Mass Spectrometry. *Sustain. Energy Fuels* **2017**, *1*, 2110–2119. [CrossRef]
36. Chen, Y.; Ren, X.; Wei, Q.; Guo, J. Hydrothermal Liquefaction of *Undaria pinnatifida* Residues to Organic Acids with Recyclable Trimethylamine. *Bioresour. Technol.* **2016**, *221*, 477–484. [CrossRef] [PubMed]
37. Hu, Y.; Wang, S.; Li, J.; Wang, Q.; He, Z.; Feng, Y.; Abomohra, A.E.; Afonaa-Mensah, S.; Hui, C. Co-Pyrolysis and Co-Hydrothermal Liquefaction of Seaweeds and Rice Husk: Comparative Study Towards Enhanced Biofuel Production. *J. Anal. Appl. Pyrolysis* **2018**, *129*, 162–170. [CrossRef]
38. Kang, S.; Li, X.; Fan, J.; Chang, J. Hydrothermal Conversion of Lignin: A review. *Renew. Sustain. Energy Rev.* **2013**, *27*, 546–558. [CrossRef]
39. Meryemoğlu, B.; Hasanoğlu, A.; Irmak, S.; Erbatur, O. Biofuel Production by Liquefaction of Kenaf (*Hibiscus cannabinus* L.) Biomass. *Bioresour. Technol.* **2014**, *151*, 278–283. [CrossRef]
40. Subramanya, S.M.; Rios, N.; Kollar, A.; Stofanak, R.; Maloney, K.; Waltz, K.; Powers, L.; Rane, C.; Savage, P.E. Statistical Models for Predicting Oil Composition from Hydrothermal Liquefaction of Biomass. *Energy Fuels* **2023**, *37*, 6619–6628. [CrossRef]
41. Wu, L.; Moteki, T.; Gokhale, A.A.; Flaherty, D.W.; Toste, F.D. Production of Fuels and Chemicals from Biomass: Condensation Reactions and Beyond. *Chem* **2016**, *1*, 32–58. [CrossRef]

Disclaimer/Publisher's Note: The statements, opinions and data contained in all publications are solely those of the individual author(s) and contributor(s) and not of MDPI and/or the editor(s). MDPI and/or the editor(s) disclaim responsibility for any injury to people or property resulting from any ideas, methods, instructions or products referred to in the content.